Experimental study of a photoelectron sheath

Adrienne Dove,[1,a)] Mihaly Horanyi,[1,2] Xu Wang,[1] Marcus Piquette,[1] Andrew R. Poppe,[3] and Scott Robertson[2]
[1]*Laboratory for Atmospheric and Space Physics, University of Colorado, Boulder, Colorado 80309, USA*
[2]*Department of Physics, University of Colorado, Boulder, Colorado 80309, USA*
[3]*Space Sciences Lab, University of California at Berkeley, Berkeley, California 94720, USA*

(Received 20 December 2011; accepted 15 March 2012; published online 4 April 2012)

We describe a set of laboratory experiments to reproduce and investigate the photoelectron layer that occurs above UV-illuminated surfaces in space. The experiments are done in vacuum with UV illumination at 172 nm that is sufficiently intense for the creation of a photoelectron layer above a large, planar metal surface with a Debye shielding distance of ~7 centimeters, small in comparison with the scale of the experiment. The emitting surface electrically floats to a potential approximately 1.5 V more positive than a nearby equipotential surface. Retarding potential analysis of the energy distribution of the electrons emitted from the electrically floating surface, as well as Langmuir probe data, show an effective electron temperature of 1.4 (±0.3) eV and a density of 4×10^{10} m^{-3}. Langmuir probe measurements are taken throughout the photoelectron sheath to determine the electron density, which show good agreement with results from a 1-D particle-in-cell simulation. These experiments enable the better understanding of the plasma environment of spacecraft, the moon, and other airless bodies in the solar system, and the processes that might be responsible for the charging, mobilization, and transport of dust particles on their surfaces. © *2012 American Institute of Physics*. [http://dx.doi.org/10.1063/1.3700170]

I. INTRODUCTION

A photoelectron sheath surrounds UV-illuminated spacecraft and airless natural bodies in space.[1] Immediately above the sunlit lunar surface, for example, the most populous species are the photoelectrons emitted from its dusty surface.[2] The photoelectrons largely determine the plasma environment of sunlit instruments on spacecraft and of instrument packages on the sunlit lunar surface. Corrections for photoelectron sheath effects are made for field and wave experiments,[3] electron energy analyzers,[4,5] and ion energy analyzers.[6,7] Electrons of spacecraft origin are easily observed[8] and must be removed from energy spectra in order to obtain the distribution of electrons of geophysical origin. In this work, we describe a series of experiments in vacuum, using 32 W of UV illumination that creates a photoelectron layer above a metal surface. Positive charging of the surface to a potential of ~1.5 V (relative to the chamber walls) is observed. Langmuir probe data taken throughout the photoelectron sheath are used to find the photoelectron density, the effective electron temperature, and the potential of the emitting surface. Data from retarding potential analysis are used to verify the electron density and temperature measurements obtained with the Langmuir probe.

A sheath is the region in a plasma adjacent to a surface in which the potential falls on the scale of the Debye length as a consequence of the space charge. Sheaths consisting only of electrons emitted from a surface were first considered in the context of thermionic vacuum tubes.[9] Electrons from heated cathodes have a temperature near 0.2 eV that is determined by the cathode temperature. Photoelectrons, in contrast, have an energy spectrum that is typically several electron volts in width, as determined by the photon spectrum and the work function of the surface.[10–12] The physics of Debye shielding in a nonneutral plasma is well-established for magnetized test particles,[13] for spherical satellites comparable in radius to the Debye shielding length,[14–16] and for flat surfaces with[17,18] and without[19] a neutralizing plasma present as a boundary condition. Theoretical modeling based on Vlasov-Poisson equations have found sheath potential profiles for spherical spacecraft[1] and above the moon modeled as a planar surface.[19–21]

Previous laboratory studies of photoelectron sheaths and the development of methods to mitigate the effects of these sheaths have been conducted in our laboratory, but were made difficult by a lack of ultraviolet sources with sufficient intensity for the observation of the photoelectric charging of surfaces and the associated space-charge electric fields. These experiments utilized a Hg-Xe arc lamp with a collimated beam to produce photoemission from surfaces.[22–25] In these experiments, photoelectrons populations were characterized with the retarding potential method and with Langmuir probes; however, there is a lack of measurements of sheath properties because of the small planar sheath geometry created by the limited photoemissive region. The present experiments have nearly uniform illumination with a radial extent three times larger than previous experiments.[25] In this configuration, the distance to an equipotential surface within the sheath is thus largely increased, and Langmuir probe data can be taken throughout the planar sheath and directly compared with results from a one-dimensional model.

This paper is organized as follows. The experiment and the diagnostic tools are described in Sec. II, and the data are presented in Sec. III. Results from particle-in-cell (PIC) code simulations and their comparison to the experimental results

[a)]Electronic mail: adrienne.dove@colorado.edu.

are presented in Sec. IV. Section V provides a discussion of these results and conclusions.

II. APPARATUS

The experiments are conducted in a cylindrical stainless steel vacuum chamber, Fig. 1, that is, 60 cm in diameter and 82 cm tall with numerous diagnostic ports arranged radially at several heights. The chamber is pumped to a base pressure of $\sim 10^{-6}$ Torr by a turbomolecular pump. Photoemission is created by an array of four vacuum-compatible Xe-excimer lamps (Osram Xeradex 20) each generating 8 W in the ultraviolet.[26] The lamps emit at a central wavelength of 172 nm with a spectral width of 14 nm FWHM. The corresponding photon energy is 7.21 eV. The UV illumination causes photoemission both from the target Zr surface and from the interior walls of the vacuum chamber.

The photoemissive surface is a 50 cm diameter disk that is covered with overlapping strips of Zr foil 12.5 cm wide. In our previous work, Zr was found to give the greatest photoemission of the materials tested (Zr, Hf, Ti, and Zn).[22,23] The surface is electrically isolated and the equipment can be operated in either one of two configurations. In the first, the surface is operated as a Langmuir probe. The bias potential of the surface is either fixed or swept in time and the current to the surface is measured. In the second configuration, the surface is connected to a high impedance voltmeter and the floating potential is recorded.

Data interpretation is complicated by the presence of photoelectrons emitted from the inner surfaces of the vacuum chamber. The relatively large interior surface area of the chamber ($\sim$2.5 m^2) emits a photoelectron current comparable to that of the Zr surface, which is an order of magnitude smaller in area but has a larger photoelectron yield. A circular nickel wire mesh grid with 74% transparency is placed above the Zr surface to define an equipotential surface. This grid is usually biased negatively to reduce the number of electrons from the chamber walls that enter the volume between the grid and the Zr surface. The wire mesh is supported by a stainless steel ring with an outer diameter of 58 cm and an inner diameter of 28 cm and is placed 7.6 cm above the Zr surface. The ring partially blocks UV illumination to the Zr surface hence only a region of $\sim$28 cm in diameter is directly illuminated. A collecting metal sheet (the "collector"), 10×15 cm, is placed vertically above the grid, near the top of the chamber, to draw in the photoelectrons from the grid and chamber surfaces without blocking the UV photons from reaching the Zr surface.

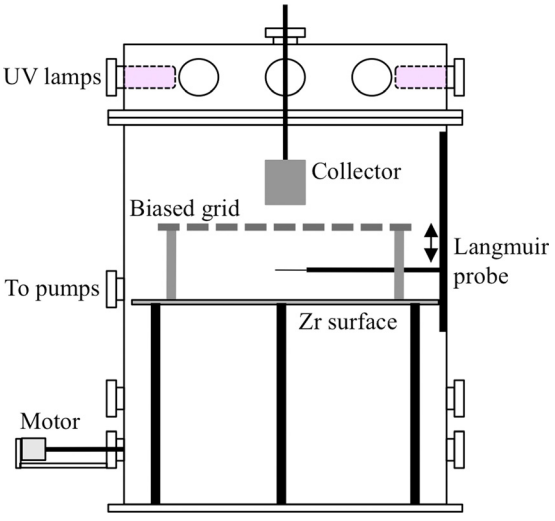

FIG. 1. The experimental apparatus. The chamber is 60 cm in diameter and 82 cm tall, and a motor moves the Langmuir probe vertically above the Zr surface. The experiment can be operated with no grid above the Zr surface, with a single grid, or with a single grid plus collector.

A. Photoemission probe

Photoelectron emission was measured as a function of distance from a single lamp using a photoelectron emission probe. This probe is a 6.25 cm^2 surface of either Pt or Zr that is operated as a Langmuir probe. Pt was used because there are accurate measurements of the photoelectron yield.[27] Zr was used for comparisons with the larger photoemissive surface. The bias voltage of the emitting probe is made lower than $\sim$3 V in order to prevent collection of photoelectrons from the chamber surfaces. Pt and Zr have work functions of 5.65 eV and 4.05 eV, respectively[28]; the work function of stainless steel walls is assumed to be approximately the same as its constituents, such as Fe (4.5–4.7 eV), Ni (5.15 eV), and Co (5.0 eV).

The Pt and Zr probes were each translated vertically beneath the center of a single lamp to measure the photoemission current as a function of distance. Fig. 2 shows the measured photoemission from the Pt, up to a distance of 17 cm, where the platinum photoemission is 1.9 μA, or 3.0 mA/m^2. For comparison, typical photoemission currents from a spacecraft surface of gold illuminated by the solar spectrum at 1 AU are $\sim 3 \times 10^{-2}$ mA/m^2, and currents from the lunar surface are in the range of 5–15 μA/m^2 from solar minima to solar maxima, respectively.[29] The quantum yield of Pt has been measured to be $\sim 9.5 \times 10^{-4}$ at 172 nm,[27] hence this current density corresponds to a photon flux of $\sim 2 \times 10^{19}$ m^{-2} s^{-1}. If we assume the lamp emits isotropically, this photon flux corresponds 8 W of emission, which agrees with the manufacturers stated power output.[26] Comparison of Zr and Pt emitters of equal area shows that the quantum yield of Zr at 174 nm is $\sim 8 \times 10^{-4}$, or $\sim$84% of the quantum yield of Pt.

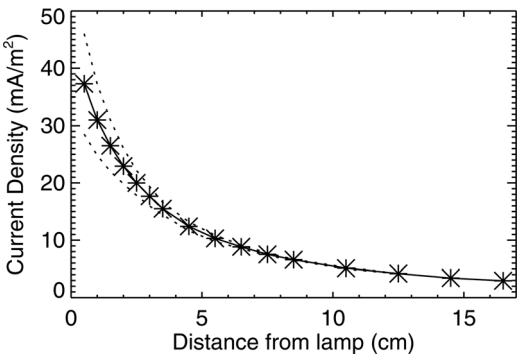

FIG. 2. Photoemission current density (mA/cm^2) from the Pt probe as a function of radial distance from a single UV lamp. Dotted lines are the range of experimental error that represents the reproducibility of the measurements.

B. Langmuir probe

The electron density and temperature are measured by a cylindrical Langmuir probe that is a nickel wire 0.5 mm in diameter and 4 cm long. Probe sweeps are controlled by computer data acquisition system, so that the probe is swept from −40 V to +20 V in increments of 0.2 V, and each data point is an average of 5000 measurements at each voltage step. The probe is regularly discharge-cleaned to minimize surface contamination. The effective electron temperature is determined by fitting a line on a semi-log plot, that is, the probe current plotted as a function of probe voltage, even though the photoelectron distribution is not necessarily Maxwellian. The density is determined from the electron saturation current, defined as the current at the voltage for which the first derivative of the I–V curve has a maximum. Photoemission from the Langmuir probe surface is less than 0.05 μA, which is negligible in comparison with the currents collected from other surfaces.

III. EXPERIMENTAL RESULTS

A. Current-voltage characteristics of the emitting surface

Photoemission from the Zr surface and from the chamber walls is characterized by measuring the electron current to or from the surface as a function of bias voltage. The current-voltage data, shown in Fig. 3(a), were taken using the same circuit that sweeps the Langmuir probe. These data, taken with no grid or collector in the chamber, show that at positive bias voltages, the surface collects a greater photoelectron current from the chamber surfaces than the surface emits when biased negatively. In order to observe the surface emission alone, the biased grid (described in Sec. II) was placed 7.6 cm above the Zr surface. This grid is biased to −20 V (relative to the grounded chamber walls) to repel electrons from the interior surfaces of the chamber. Electrons from the chamber walls can have energies greater than the difference between the photon energy and the work function of the metal surface as a consequence of contamination. The walls have patches of insulating contamination which will charge negatively.[30] Electrons emitted from negative surfaces have their kinetic energies increased when they enter regions with electrostatic potentials that are more positive. Thus, the grid bias voltage of −20 V is necessary to repel the electrons from the chamber, which is much more negative that one would estimate from the photon energy and work functions. Additionally, the collector (described in Sec. II) is placed ∼5 cm above the grid and biased to +60 V to collect electrons from the chamber surface that would otherwise enter the region between the Zr surface and the grid. This collector is more positive than the grid and thus also attracts photoelectrons emitted from the grid itself. Voltage sweeps with both the biased grid and collector in place show that the current emitted by the Zr surface approaches a constant value of 65 μA as the surface bias voltage is made more negative. (Note that the horizontal axis in Fig. 3(a) is the Zr surface voltage relative to the −20 V on the grid.) This relatively constant current is the photoemission current from the Zr surface with negligible contribution from the electrons from the walls.

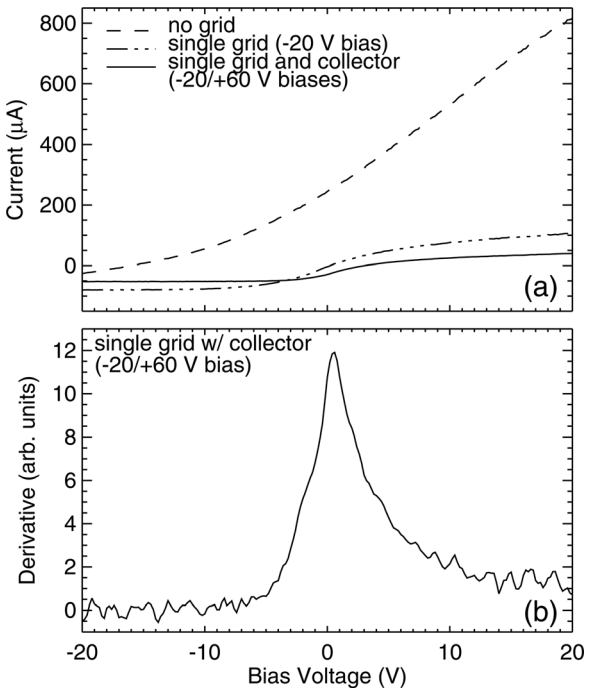

FIG. 3. (a) Zr surface current as a function of bias voltage without a grid, with a single grid, and with a grid and biased collector to partially remove electrons emitted by the walls and the grid. The grid is biased to −20 V, and for the case of the grid plus collector, the collector is biased to +60 V. Sweeps are plotted as a function of the grid bias for these cases. (b) Derivative of the current for the Zr surface sweep with a grid and collector in the chamber.

The Zr surface–Ni grid combination acts as a retarding potential analyzer. For example, with the surface 1 V more positive than the grid, electrons emitted perpendicularly from the surface with more than 1 eV of energy are able to pass through the grid. The cutoff energy varies as the surface is swept; hence the derivative is a measure of the axial energy distribution function. With the surface 1 V more negative than the grid, photoelectrons from the grid and other nearby surfaces are repelled from the Zr surface, and the derivative is a measure of energy distribution of these "contaminating" electrons. The electrons with many tens of electron volts of energy that come from the negative surfaces of the grid and the walls have a broad distribution and the derivative of this distribution is small relative to that of the photoelectrons from clean surfaces. The half-width at the half maximum, Fig. 3(b), is about 3 V, which is comparable to the maximum photoelectron energy of 3.16 eV that is calculated from the difference between the photon energy (7.21 eV) and the Zr work function (4.05 eV).

For an illuminated area with a diameter of 28 cm, the emission current from the electrically floating Zr surface, J_{ph}, is ∼0.78 mA/m^2 (Table I). From this measurement, we also determined an emitted photoelectron temperature, T_e, by fitting the slope of the linear portion of the current on a semi-logarithmic plot as is done for the Langmuir probe. For the case of the single grid plus collector, we measured $T_e = 1.75 \pm 0.9$ eV. We assume the photoelectrons are moving with a mean axial velocity, $v = \sqrt{2kT_e/\pi m_e}$. Thus, the density of photoelectrons emitted from the surface is

TABLE I. Photoelectron sheath parameters derived (1) from sweeps of the Zr surface and (2) from Langmuir probe sweeps taken with the Zr surface floating.

	V_f (V)	V_p (V)	J_{pe} (mA/m^2)	kT_e (eV)	n_e ($\times 10^{10}$ m^{-3})	l (cm)
1. Surface sweep	−16.8	−19.2	0.78	1.75	2.46	5.12
2. Probe sweep	−16.8	−16.2	0.47	1.03	3.99	3.08

approximately $n_0 = 2J_{ph}/qv = 2.5 \times 10^{10}$ m^{-3} with a Debye shielding distance of 5.12 cm; this distance is less than the spacing between the Zr surface and the grid.

A photoemitting surface in vacuum will electrically float to the potential that returns all the photoemitted electrons. For a Zr surface illuminated with 7.2 eV photons, this potential is +3.05 V. In the experiment, photoelectrons from other surfaces are incident upon the Zr surface and the floating potential has the value that balances the currents to and from its surface. The nearest surface to the Zr surface is the grid, thus, in the absence of photoelectrons from other surfaces, the surface should float to a potential ∼3 V more positive than the grid potential. Fig. 4 shows the potential of the surface relative to the grid for a range of grid bias voltages. The surface potential is determined by two methods: (1) a high impedance (∼1 GΩ) voltmeter; and (2) by sweeping the surface and determining when the current is zero. These two methods agree to within ±0.2 V. The data show that the floating potential approaches +1.5 V as the grid potential is made more negative to reduce the contribution of electrons from the walls. Hence at this potential, the photoemission current is equal to the current of photoelectrons that pass through the grid or are emitted from the grid.

B. Langmuir probe data

Cylindrical Langmuir probe I-V traces and their derivatives are shown in Fig. 5 for the standard experimental setup with a grid and collector above the biased Zr surface and the probe placed 4 mm above the Zr surface. When the probe is biased to ≤−30 V, the measured current is primarily an emission current produced by photoemission from the probe[25]; in Fig. 5(a), it is evident that, for most cases, the probe emits significantly less than the photocurrent collected from the Zr surface. Although the plasma consists solely of electrons, we use the orbit-motion-limited (OML) theory[31] for analysis of the Langmuir probe data because the validity of the theory is not dependent upon the presence of ions.

Fig. 5(a) shows that the current collected by the probe is greatest when the surface bias is the most positive relative to the grid, which is the condition that returns photoelectrons to the Zr surface and results in an electron distribution function that is nearly symmetric about zero velocity. For these conditions, the electron temperature from the probe analysis is 1.28 eV and the density is 4.35×10^{10} m^{-3}. As shown in Table II, the density of photoelectrons just above the surface, as measured by the Langmuir probe, decreases as the surface is made more negative.

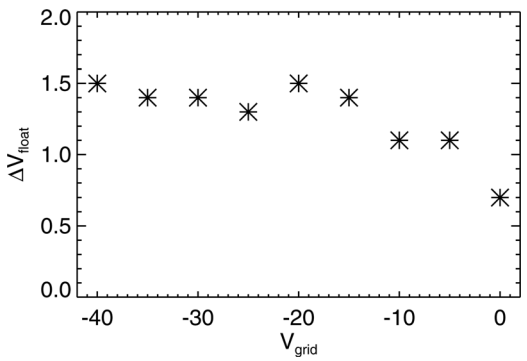

FIG. 4. The floating potential of the Zr surface is determined by sweeping the voltage on the surface itself and determining the voltage where the current goes to zero. Data points are the voltage difference between the measurements and the grid potential.

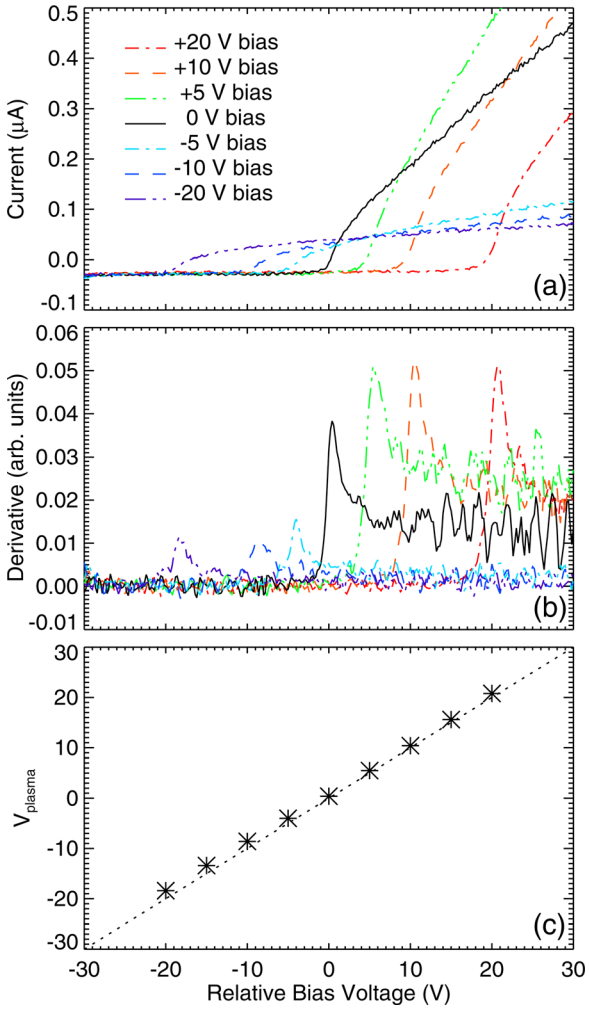

FIG. 5. (a) Cylindrical Langmuir probe sweeps taken ∼4 mm above the Zr surface; voltages are measured relative to the −20 V biased grid, with data plotted for surface bias voltages from +20 to −20 V. (b) Derivatives of the sweeps shown in (a). (c) Plasma potential at the probe location, determined from the peak in the first derivatives of the voltage sweeps.

TABLE II. Photoelectron temperature and density data determined from Langmuir prove sweeps taken ~4 mm above the biased Zr surface. The surface bias is given with respect to the −20 V grid bias.

Bias (V)	kT_e (eV)	n_e ($\times 10^{10}$ m^{-3})	l (cm)
+20	1.28	4.35	3.29
+10	1.11	3.64	3.35
+5	1.06	3.82	3.20
0	1.06	2.26	4.16
−5	1.55	0.96	7.72
−10	2.0	0.94	8.86
−20	1.64	0.80	8.70

First derivatives of the probe data are shown in Fig. 5(b). The peak in the first derivative is identified as the plasma potential in probe data from plasma of electrons and ions. For the photoelectron data, the peak in the first derivative of the probe data is observed to be at a voltage that is always slightly above the bias potential on the emitting surface. This point is shown more clearly in Fig. 5(c), where the location of the peak is plotted as a function of the surface bias. A detailed analysis shows that, except for very positive biases, the peak is always about 1.4 V more positive than the surface potential. Future efforts will attempt to utilize an emissive probe as an additional measurement of the potential throughout the sheath. These efforts have thus far been impeded due to the fact that the probe emission produces a large perturbation in the low density photoelectron sheath.

In Table I, the temperatures and densities derived from the floating surface sweeps are shown to be different than those derived from the Langmuir probe sweeps. Electron density is related to the probe current and electron temperature by the expression $J = n_e q\sqrt{T_e/2\pi m_e}$, where T_e is in eV and n_e is the density of electrons. This population of electrons is measured by the probe just above the surface and can be treated as a two-sided Maxwellian distribution because the electrons are emitted from and returning to the surface, effectively doubling the measured density. This effect also explains why the densities measured by the probe (Table II) increase with positive surface voltages. When the surface is biased to −20 V, the density is reduced because the electrons are accelerated away.

IV. DENSITY PROFILES IN PHOTOELECTRON SHEATHS

Langmuir probe measurements are taken throughout the volume of the photoelectron sheath, and the data are used to derive the electron density at each height. To gain a more complete understanding of these measurements, we simulated the photoelectron sheath between the Zr surface and Ni grid using a 1-D PIC code (described in detail in Ref. 32). Emission from the Zr surface was simulated by defining a photoelectron current density such that the surface emits a Maxwellian distribution of photoelectrons with a defined $T_{e,Zr}$. Grid emission is defined as a given percentage of the surface current density and a specified $T_{e,grid}$. For this work, the current density of photoelectrons emitted from the Zr surface, determined from the experimentally measured photoemission current, is $J_{ph} = 0.9$ mA/m^2, emission from the grid is 10% of the surface photoelectron current density, and $T_{e,Zr} = T_{e,grid} = T_e = 1.75$ eV. Although the surface and grid electron populations are not expected to have exactly the same effective T_e, they are expected to be between 1 and 2 eV, and a value of $T_e = 1.75$ eV fits the measured densities well. The voltage on the grid was fixed at −20 V and the bias on the Zr surface boundary was varied between 0 V and −40 V, as in the experiments.

When the surface is biased very positively with respect to the grid, as illustrated in Fig. 6(a), the surface photoelectrons are returned to the surface and the grid electrons are drawn toward the surface, so that a Langmuir probe positioned just above the Zr surface will measure contributions from both populations. When the surface is very negatively biased, photoelectrons from the Zr surface are drawn toward the grid and grid photoelectrons do not reach the surface, so that a Langmuir probe just above the surface will primarily measure the surface photoelectron population. Fig. 6(b) graphically illustrates the change in electron density due to the changing surface bias. In the case of the positively biased Zr surface, the density just above the surface will be about 2.5 times higher than that expected from a photoelectron population with only upward-directed motion, due to the returning photoelectron population and the contribution from grid electrons. However, with the surface negatively biased, the density increases about 2.5 times just below the equipotential grid and falls to the expected value just above the surface.

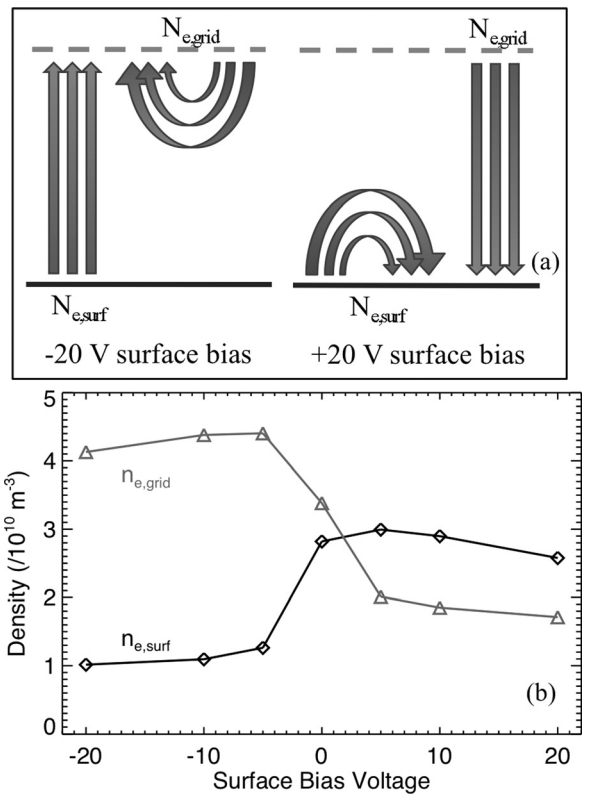

FIG. 6. (a) Cartoon illustrating the effect of surface bias potential on the photoelectron populations. (b) Results from the 1-D PIC simulations showing the difference in densities at the Zr surface and the grid as a function of surface bias potential.

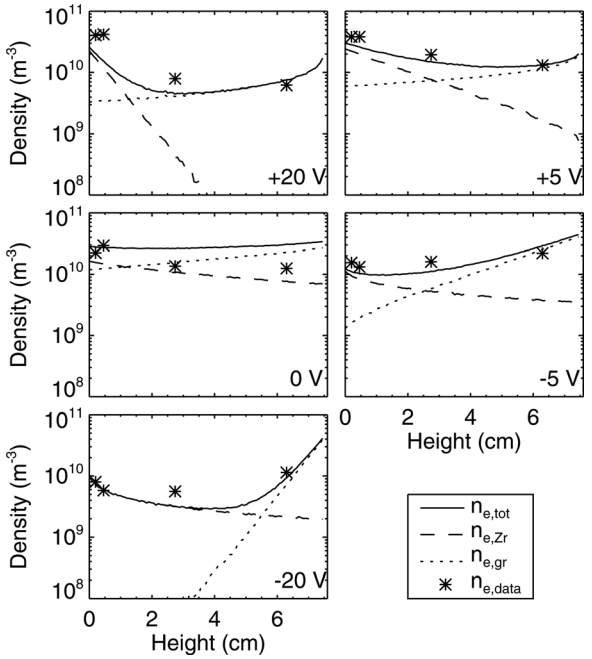

FIG. 7. Comparisons of the electron densities from 1-D PIC simulations with experimental measurements asterisks derived from Langmuir probe sweeps taken at four locations between the surface and the grid. The given surface bias relative to the grid bias (−20 V) is shown in each plot. Each of the simulations has the same emission current from the Zr surface, $J_{e,Zr} = 9 \times 10^{-4}$ A/m^2, with emission from the grid, $J_{e,gr}$ set to 10% of the Zr surface emission, and $T_e = 1.75$ eV for the photoelectrons from both the grid and Zr surface.

In Fig. 7, electron densities derived from Langmuir probe data are compared directly with PIC simulation results, which can be broken down into components from both the surface and the grid. Overall, the measured and predicted densities show good agreement. When the surface and grid are at the same bias (Fig. 7, 0 V), the predicted density profile is relatively flat due to the extended Debye length; the measured densities decrease only slightly toward the grid. The data has a slight discrepancy with the simulations near the very positively biased surface. This is likely a measurement effect due to the increased electron population as a result of photoelectrons returning to, and grid electrons being drawn toward, the more positive surface.

V. DISCUSSION AND CONCLUSION

The characteristics of photoelectron sheaths that occur at surfaces in space have been studied in the laboratory using a large planar surface of Zr illuminated by four Xe-excimer lamps each generating 8 W at 172 nm. Electron densities are measured in the photoelectron sheath between the emitting surface and a grid spaced 7.6 cm above the surface that is used to repel electrons emitted from the chamber walls. The surface-grid combination is operated as a retarding potential analyzer to determine the photoelectron density ($\leq 4.3 \times 10^{10}$ m^{-3}) and temperature (1-2 eV). The Debye shielding distance (~7 cm) is comparable to the surface-grid separation, thus, the entire area between the surface and grid can be probed to understand the sheath physics. Langmuir probe data, analyzed by OML theory, give temperatures and densities within a factor of two of those from retarding potential analysis. A PIC simulation was used to simulate the sheath, including the electrons originating at the Zr surface and at the grid. These simulations show that the change in photoelectron density with grid bias is explained by photoelectrons from the surface being returned to the surface by a retarding potential and by photoelectrons from the grid. Densities measured throughout the sheath by the Langmuir probe are comparable to PIC simulation results. These experiments demonstrate the use of a Langmuir probe to determine the characteristics of the photoelectron sheath above a surface, which aid in the interpretation of measurements of photoelectrons above surfaces in space; based on this work, signals from photoelectron populations can be isolated from signals from electrons of geophysical or solar origin.

ACKNOWLEDGMENTS

This work is supported by the NASA Lunar Science Institute's Colorado Center for Lunar Dust and Atmospheric Studies at the Laboratory for Atmospheric and Space Physics, University of Colorado at Boulder. Additional support was provided by a NASA Graduate Student Research Program fellowship awarded to A. Dove. We wish to thank an anonymous reviewer for useful comments and insight which improved the manuscript.

[1]E. Whipple, "Potentials of surfaces in space," Rep. Prog. Phys. **44**, 1197–1250 (1981).
[2]J. E. Colwell, S. Batiste, M. Horányi, S. Robertson, and S. Sture, "Lunar surface: Dust dynamics and regolith mechanics," Rev. Geophys. **45**, RG2006, doi:10.1029/2005RG000184 (2007).
[3]C. M. Cully, R. E. Ergun, and A. I. Eriksson, "Electrostatic structure around spacecraft in tenuous plasma," J. Geophys. Res. **112**, A09211, doi:10.1029/2007JA012269 (2007).
[4]E. E. Scime, J. L. Phillips, and S. J. Bame, "Effects of spacecraft potential on the three-dimensional electron measurements of the solar wind," J. Geophys. Res. **99**, 14769–14776, doi:10.1029/94JA00489 (1994).
[5]J. D. Scudder, X. Cao, and F. S. Mozer, "Photoemission current-spacecraft voltage relation: Key to routine, quantitiative low-energy plasma measurements," J. Geophys. Res. **105**, 21281–21294, doi:10.1029/1999JA900423 (2000).
[6]C. Olsen, "The hidden ion population of the magnetosphere," J. Geophys. Res. **87**, 3481–3488, doi:10.1029/JA087iA05p03481 (1982).
[7]J. J. Sojka, G. L. Wrenn, and J. F. E. Johnson, "Pitch angle properties of magnetospheric thermal protons and satellite sheath interference in their observation," J. Geophys. Res. **89**, 9801–9811, doi:10.1029/JA089iA11p09801 (1984).
[8]S. Szita, A. N. Fazakerley, P. J. Carter, A. M. James, P. Trávnícek, G. Watson, M. André, and K. Torkar, "Cluster peace observations of electrons of spacecraft origin," Ann. Geophys. **19**, 1721–1730 (2001).
[9]L. Tonks and I. Langmuir, "A general theory of the plasma of an arc," Phys. Rev. **34**, 876–922 (1929).
[10]R. J. L. Grard, in *Photon and Particle Interactions with Surfaces in Space, 6th ESLAB Symposium* (Springer, New York, 1973), Vol. 37.
[11]R. J. L. Grard, "Properties of the photoelectron sheath derived from photoemission laboratory measurements," J. Geophys. Res. **78**, 2885–2906, doi:10.1029/JA078i016p02885 (1973).
[12]B. Feuerbacher, B. Fitton, and R. F. Willis, *Photoemission and the Electronic Properties of Surfaces* (Wiley, 1978).
[13]R. C. Davidson, "Electrostatic shielding of a test charge in a non-neutral plasma," J.Plasma Phys. **6**, 229–235 (1971).
[14]H. Schröder, "Spherically symmetric model of the photoelectron sheath for moderately large plasma Debye lengths," in *Photon and Particle Interactions with Surfaces in Space*, edited by R. J. L. Grard (Astrophysics and Space Science Library, 1973), Vol. 37, pp. 51–58.
[15]J. K. E. Tunaley and J. Jones, "The photoelectron sheath around a spherical body," in *Photon and Particle Interactions with Surfaces in Space*,

edited by R. J. L. Grard (Astrophysics and Space Science Library, 1973), Vol. 37, p. 59.
[16]J. E. C. Whipple, "Theory of the spherically symmetric photoelectron sheath: A thick sheath approximation and comparison with the ats 6 observation of a potential barrier," J. Geophys. Res. **81**, 601–607, doi:10.1029/JA081i004p00601 (1976).
[17]R. L. Guernsey and J. H. M. Fu, "Potential distribution surrounding a photo-emitting plate in a dilute plasma," J. Geophys. Res. **75**, 3193–3199, doi:10.1029/JA075i016p03193 (1970).
[18]J. H. M. Fu, "Surface potential of a photoemitting plate," J. Geophys. Res. **76**, 2506–2509, doi:10.1029/JA076i010p02506 (1971).
[19]R. J. L. Grard and J. K. E. Tunaley, "Photoelectron sheath near a planar probe in interplanetary space," J. Geophys. Res. **76**, 2498–2505, doi:10.1029/JA076i010p02498 (1971).
[20]S. F. Singer and E. H. Walker, "Photoelectric screening of bodies in interplanetary space," Icarus **1**, 7–12 (1962).
[21]E. Walbridge, "Lunar photoelectron layer," J. Geophys. Res. **78**, 3668–3687, doi:10.1029/JA078i019p03668 (1973).
[22]A. A. Sickafoose, J. E. Colwell, M. Horányi, and S. Robertson, "Photoelectric charging of dust particles in vacuum," Phys. Rev. Lett. **84**, 6034–6037 (2000).
[23]A. A. Sickafoose, J. E. Colwell, M. Horányi, and S. Robertson, "Experimental investigations on photoelectric and triboelectric charging of dust," J. Geophys. Res. **106**, 8343–8356, doi:10.1029/2000JA000364 (2001).
[24]X. Wang, M. Horányi, Z. Sternovsky, S. Robertson, and G. E. Morfill, "A laboratory model of the lunar surface potential near boundaries between sunlit and shadowed regions," Geophys. Res. Lett. **34**, L16104, doi:10.1029/2007GL030766 (2007).
[25]X. Wang, M. Horányi, and S. Robertson, "Plasma probes for the lunar surface," J. Geophys. Res. **113**, A08108, doi:10.1029/2008JA013187 (2008).
[26]*XERADEX lamp manual version 1.5 ed.*, OSRAM SYLVANIA, Inc., Danvers, MA, 2009.
[27]S. F. Lin, D. T. Pierce, and W. E. Spicer, "Photoemission studies of platinum," Phys. Rev. B **4**, 326–329 (1971).
[28]H. B. J. Michaelson, "The work function of the elements and its periodicity," J. Appl. Phys. **48**, 4729–4733 (1977).
[29]Z. Sternovsky, P. Chamberlin, M. Horányi, S. Robertson, and X. Wang, "Variablility of the lunar photoelectron sheath and dust mobility due to solar activity," J. Geophys. Res. **113**, A10104, doi:10.1029/2008JA013487 (2008).
[30]S. Robertson, Z. Sternovsky, and B. Walch, "Reduction of asymmetry transport in the annular penning trap," Phys. Plasmas **11**, 1753–1756 (2004).
[31]J. H. Mott-Smith and I. Langmuir, "The theory of collectors in gaseous discharge," Phys. Rev. **28**, 727–763 (1926).
[32]A. Poppe and M. Horányi, "Simulations of the photoelectron sheath and dust levitation on the lunar surface," J. Geophys. Res. **115**, A08106, doi:10.1029/2010JA015286 (2010).